Article

Journal of the Brazilian Chemical Society

https://dx.doi.org/10.21577/0103-5053.20240123

J. Braz. Chem. Soc. **2025**, *36*, 2, e-20240123, 1-12

Thermal and Mechanical Evaluations of Innovative Polyurethane Materials and Its Precursors Based on *Moringa oleifera* Oil

Kamilla B. Silveira,[a,b,c] Gabriel E. P. Almeida,[c] Debora H. A. Brito,[c] Francisco-Alessandro M. Rodrigues,[c] Elano N. Ferreira,[c] Adriano L. A. Mattos,[d] Denise R. Moreira,[c] Alexandre C. C. Sousa,[c,e] Douglas Britto[d] and Nágila M. P. S. Ricardo *,[c]

[a]*Instituto de Ciência dos Materiais, Universidade Federal do Vale do São Francisco (UNIVASF), 48902-300 Bahia-BA, Brazil*

[b]*Instituto Federal do Sertão Pernambucano, 56316-686 Pernambuco-PE, Brazil*

[c]*Laboratório de Polímeros e Inovação de Materiais, Departamento de Química Orgânica e Inorgânica, Universidade Federal do Ceará (UFC), 60020-181 Ceará-CE, Brazil*

[d]*Laboratório de Biomassa, Embrapa Agroindústria Tropical, 60511-110 Ceará-CE, Brazil*

[e]*Instituto Federal de Educação, Ciência e Tecnologia do Ceará (IFCE), Campus Quixadá, 63902-580 Ceará-CE, Brazil*

This study highlights the synthesis of innovative polyurethane materials derived from *Moringa oleifera* oils extracted from two distinct sources. The oils were converted into their respective polyols through the *in situ* generated performic acid method. Diverse material characteristics were observed due to different agroclimatic and cultivation conditions for the sources. Extraction yields were 45.21% (source 1) and 40.32% (source 2), with acid values of 28.70 and 26.00 mg KOH *per* g of oil, respectively. Oleic acid constituted 79.87 and 67.11% of the oils composition, respectively. Nuclear magnetic resonance and Fourier transform infrared spectroscopy (FTIR) confirmed the hydroxylation of the oils. FTIR also identified the isocyanate structures in the synthesized polyurethane materials. Gel permeation chromatography analysis revealed a higher oligomer content in the polyol synthesized from the oil extracted from source 2. Thermogravimetric analysis demonstrated enhanced thermal stability post-oil conversion, highlighting decomposition stages for rigid and flexible segments. Differential scanning calorimetry indicated higher unsaturation in the oil extracted from source 1, resulting in an elevated crystallization temperature. Tensile testing showed increased elasticity as the [NCO]/[OH] ratio decreased in the material, emphasizing the influence of polyol and crosslinking agent concentrations on mechanical resistance of polyurethane materials.

Keywords: polyurethane, bio-polyol, *Moringa oleifera*, thermal stability, mechanical resistance

Introduction

Bio-based polymers have attracted a lot of attention in recent decades, due to the current demand for green materials that are economically and environmentally viable and with characteristics that allow them to replace existing conventional petrochemical-based polymers.[1] Polyurethanes, for example, have undergone a significant shift from conventional petroleum-based raw materials to various renewable alternatives, such as vegetable oils, fatty acids, carbohydrates, proteins, starch, cellulose, polysaccharides and many other agricultural products and by-products. Among the broad spectrum of research into renewable raw materials, vegetable oil is undoubtedly a more advantageous and promising alternative to petrochemical resources.[2] The main achievement in this regard is devoted to the property of polyol from vegetable oils.[3] The scientific literature reports[4] the preparation of polymers from soybean, linseed, sunflower, palm, cotton and castor oils through

*e-mail: naricard@ufc.br
Editor handled this article: Fernando C. Giacomelli (Associate)

synthetic routes that involve reactions, such as epoxidation, transesterification or acrylation.

Moringa oleifera is an Indian tree, now widely cultivated in many countries in Asia, South America and Africa.[5] Its interest in agro-industrial purposes is due to a fast-growing cork oak, good tolerance to arid soils and its easily adaptable to the different climates of Brazil. Currently, its distribution is cosmopolitan, occurring mainly in tropical and subtropical regions. In Brazil, its spread occurs during all times of the year, mainly in the Northeast region due to its adaptation to arid and semi-arid climates.[6,7] *Moringa oleifera* seed grains contain 35 to 40% oil, with a high oleic content, about 70%, and a small amount of essential fatty acids such as linolenic acid (0.2%) and linoleic acid (0.77%).[6,8] Oleic acid is a fatty acid composed of eighteen carbons (C18), containing a carbon-carbon double bond in the ninth position, whose chemical structure has polymerization potential through preliminary preparation of polyols and their subsequent polycondensation with diisocyanates, since the polymerization of unsaturated oils can be obtained by taking advantage of the carbon-carbon double bonds from the oils chemical structure.[6,7,9,10] In the epoxidation route, vegetable oil undergoes an intermediate process in which a highly unstable epoxide is formed. Under strongly acidic conditions, *in situ* ring opening occurs, resulting in the formation of the hydroxyl group.[3] Genetic, climate, seasonal, and agronomic factors can impact the quality and quantity of vegetable oils, including those from moringa seeds.[7]

This study aims to produce polyols from *Moringa oleifera* oil (MO) sourced from two different origins, employing the oxirane ring opening technique for hydroxylation. These polyols are then utilized in the synthesis of polyurethane materials using toluene diisocyanate (TDI) at varying [NCO]/[OH] ratios. Chemical modifications were tracked using infrared spectroscopy (IR), nuclear magnetic resonance (^{1}H NMR), and gel permeation chromatography (GPC). Additionally, the thermal and mechanical properties of the resulting polyurethanes were assessed. Variations in agroclimatic and cultivation conditions for the two selected sources led to distinct material characteristics. However, further investigation is needed to identify the specific relationship between agroclimatic factors and the chemical composition of the extracted oils from moringa seeds.

Experimental

Materials

Moringa oleifera source 1 seeds were collected from plants grown on the university campus (Campus do Pici) located in Fortaleza city, Ceará, Brazil (3°44'21.4"S 38°34'29.3"W) while the seeds from *Moringa oleifera* source 2 were collected from Petrolina city, Pernambuco, Brazil (9°22'47.6"S 40°31'37.4"W). *n*-Hexane and hydrogen peroxide (39%) were purchased from LabSynth (São Paulo, Brazil). Toluene diisocyanate (80% 2,4-TDI isomer, 99% purity) and formic acid ≥ 98% were purchased from Sigma-Aldrich (Saint Louis, USA).

Seed processing and oil extraction

The oils were named MO1 (extracted from *Moringa oleifera* source 1 seeds) and MO2 (extracted from *Moringa oleifera* source 2 seeds). The seeds were manually collected, separated from the outer layer, and processed in a blender. The resulting material was sieved through a series of Tyler sieves (20), selecting the fraction with a granulometry close to 0.850 mm. Approximately 150 g of this fraction were added to a 2 L Soxhlet extractor, connected to a reflux system equipped with a cooling bath, and extracted with *n*-hexane at a liquid-to-solid ratio of 10:1. The extraction was performed at 60 ºC for 6 h after the initial extraction. The solvent was separated from the oil using vacuum evaporation.[5,11]

Polyol production

Moringa oleifera oil was weighed and placed in a 500 mL round-bottom flask. Formic acid was gradually added with a molar ratio of double bonds to formic acid at 1:3, under vigorous stirring. Subsequently, hydrogen peroxide (29%, molar ratio of double bonds to hydrogen peroxide 1:1.5) was slowly introduced through an addition funnel over 1 h. The mixture was heated between 65 to 70 °C for 4 h. Then, a 100 mL solution of sodium bisulfite (10%) was added, to guarantee the discontinuation of the hydroxylation process through the peroxide consumption.[12] The resulting mixture formed two layers, which were separated. The organic phase was washed with distilled water (3 times) and saturated with sodium chloride solution (2 times). The remaining water was eliminated using a rotary evaporator.[13] Polyols synthesized from MO1 were called PMO1, while the polyols synthesized from MO2 were called PMO2.

Polyurethane synthesis

For comparison purposes, polyurethanes materials (PUs) were prepared using different [NCO]/[OH] ratios. For the PUs synthesized from PMO1 (PU1) the molar ratios tested were 0.4, 0.6, 0.8 and 1.0. After interpreting these results, it was adopted the molar ratios of 1.0 and 1.2 for

the PUs synthesized from PMO2 (PU2). After adding TDI to the polyol, the mixtures were stirred at approximately 3.000 rpm for 1 min. The resulting mixtures were poured into polytetrafluoroethylene molds and cured in an oven at 60 °C for 24 h.[12]

Gas chromatography-mass spectrometry (GC-MS)

The extracted oils were analyzed by GC-MS Shimadzu (Kyoto, Japan) QP-2010 ULTRA, equipped with a (5%-phenyl)-methylpolysiloxane (DB-5) capillary column (30 m × 0.25 mm), using helium as carrier gas (at flow rate of 0.6 mL min^{-1}) in splitless mode (injection volume 1 µL, of 1 mg mL^{-1} solutions with ethyl acetate). The oven temperature was initially set at 120 °C and programmed for 10 °C min^{-1} up to 300 °C, then maintained for 10 min. The injector and detector temperatures were, respectively, 250 and 300 °C. The quadrupole analyzer was set to electron ionization (EI) and scanned in a range between 50 and 450 *m/z*.

Gel permeation chromatography (GPC)

The weighted average molar mass (Mw) and the number average molar mass (Mn) of the polyols were determined using a Shimadzu (Kyoto, Japan) high-performance liquid chromatograph (HPLC), with a RID-10A refractive index detector, using a pre-column and two columns in series Phenomenex-GPC/SEC linear 7.8 × 300 mm, 5 µm, tetrahydrofuran (THF) mobile phase at 40 °C, flow rate of 1 mL min^{-1}, flow time of 25 min. The samples were prepared in 1 mg mL^{-1} THF, solubilized under constant stirring for 60 min and then filtered through a 0.45 µm Millipore membrane. The injected sample volume was 20 µL and the standard curve was polystyrene with known Mw (from 1.22×10^3 to 6.25×10^5 g mol^{-1}).

^{1}H nuclear magnetic resonance (NMR) spectroscopy

The oils and polyols obtained were analyzed through ^{1}H NMR (8 transients) on a Bruker Avance DRX 500 MHz Spectrometer (Karlsruhe, Germany). 20 mg of the sample were dissolved in 0.5 mL of deuterated chloroform ($CDCl_3$) and the spectra were analyzed using the MestReNova software.[14]

Spectroscopy in the Fourier transform infrared (FTIR) region

FTIR spectra of oil, polyols, and uncured PUs were obtained by a 620-IR spectrometer (Varian, Inc., USA) in attenuated total reflection (ATR) mode with selenide crystal. The scan was performed in the range of 4000 to 600 cm^{-1}. For cured PU samples, FTIR infrared spectra were performed by a 16 PC spectrometer (PerkinElmer, Norwalk, USA) on KBr pellets, in the range of 4000 to 400 cm^{-1}, from fragments obtained by sanding.[15]

Thermogravimetric analysis (TGA)

The thermal stability of the oil, polyol and PUs samples was analyzed using a Shimadzu (Kyoto, Japan) DTG-60H differential thermogravimetric/thermal analysis equipment operating in an inert nitrogen atmosphere, at a heating rate of 10 °C min^{-1}, flow of 40 mL min^{-1}, with a heating range from 25 to 1000 °C. Approximately 4.52 ± 0.32 mg of oil, 6.54 ± 0.85 mg of polyol, and 7.46 ± 0.32 mg of PU were used on an alumina support as a gate sample.

Differential scanning calorimetry (DSC)

DSC analyses of oil, polyol and PU samples were carried out using a DSC Q20 model equipment (TA Instruments, New Castle, USA) at Embrapa Agroindústria Tropical in Fortaleza. DSC curves were obtained in the temperature range of –90 to 250 °C, under a nitrogen atmosphere, flow of 50 mL min^{-1} and heating rate of 10 °C min^{-1}.

Mechanical tensile test

The PU tensile test was carried out by an Universal Testing Machine, model DL3000, EMIC INSTRON (São José dos Pinhais, Brazil). The test speed was 10 mm min^{-1} and the applied tensile strength was 500 N. The test specimens were cut into a dumbbell shape with a length of 15 mm and a narrow section width of 2 mm.

Results and Discussion

Characterization of the *Moringa oleifera* extracted oils (MO1 and MO2) and their respective converted polyols (PMO1 and PMO2)

The extraction process yielded 45.21% for MO1 and 40.32% for MO2, with an acid number of 28.70 ± 1.00 and 26.00 ± 1.6 mg KOH *per* g_{oil}, respectively.

Confirmation of the fatty acid composition through GC-MS analysis revealed oleic acid as the predominant fatty acid in both compositions, with percentages of 78.32 and 60.55%, respectively (Table S1, Supplementary Information (SI) section). The structure of the oils was characterized by FTIR, with the main bands of the triglyceride functional groups highlighted (Figure 1).

The strong signal at 1743 cm^{-1} was attributed to the C=O stretching of the triglyceride ester groups. The weak absorption band (one shoulder) at 3008 cm^{-1} corresponded to the C–H elongation vibration of the aliphatic C=C–H group, while the very small band at 1656 cm^{-1} was attributed to the C=C elongation vibration in *cis* conformation.[16] Due to the relatively high acidity of *Moringa oleifera* oil, it is possible to verify the small band at 1710 cm^{-1} referring to the stretching vibration of the carboxylic acid carbonyl.[17] However, in MO1 this band is clearly more intense than in MO2. The presence of water in the rainy season extracts promoted an increase in free fatty acids due to the hydrolysis reaction. Water (a weak nucleophile) attacks the ester bond of triacylglycerols generating mono-diacylglycerols, in addition to glycerol and free fatty acids.[7]

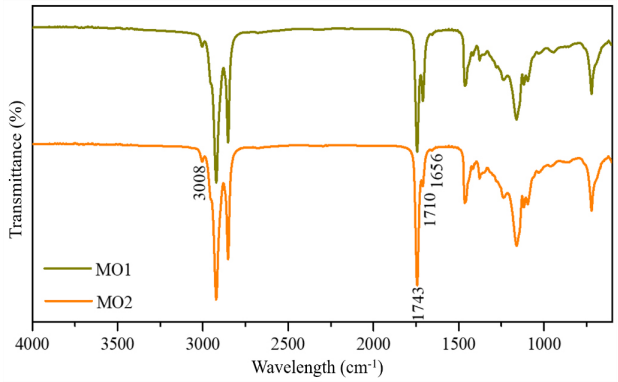

Figure 1. FTIR-ATR spectra obtained for MO1 and MO2.

The mechanistic proposal for the triglyceride hydroxylation reaction using the *in situ* generated performic acid method and the structural representation of the product are shown in Figures S1 and S2 in the SI section. The obtained PMO1 appeared as a clear and very viscous liquid, while PMO2, a white waxy solid at room temperature (Figure S3, SI section). Polyols typically exhibit high viscosity (when in polymer form) or solidity (when of low molecular weight) at room temperature, due to hydrogen bonding. According to Pan and Webster,[18] the conversion of epoxy groups to hydroxyl groups increases the viscosity due to increased hydrogen bonds, however, oligomerization can lead to a significant increase in the viscosity of polyols. Furthermore, Kong *et al.*[19] explain that higher degrees of hydrolysis result in a product with a higher hydroxyl content and lower viscosity, when compared to the oligomerization process, which results in a lower hydroxyl content and higher viscosity. Hence, we can deduce that the decreased viscosity of PMO1 stems from its higher degree of hydrolysis and lower degree of oligomerization. To compare and calculate the [NCO]/[OH] molar ratio used in the polymerization reactions, the hydroxyl index (ASTM D1957-86)[20] of the precursor polyols was checked: PMO1 171.06 mg KOH *per* g of sample and PMO2 176.97 mg KOH *per* g of sample.

To qualitatively confirm the successful conversion of *Moringa oleifera* oils into their corresponding polyols (PMO1 and PMO2), the attenuated total reflectance Fourier transform infrared (ATR-FTIR) technique was employed (Figure 2). The presence of the bands at 3451 cm and 1726 cm^{-1} of the hydroxyl group stretching vibration and ester group carbonyl stretching, respectively, evidenced the formation of polyols.[21] The presence of hydroxyl in the polyol was also reflected by the 1101 cm^{-1} band, due to secondary alcohol hydroxyl stretching. The carbonyl stretch at 1743 cm^{-1}, attributed to the presence of the moringa oil ester bond, was slightly shifted to 1726 cm^{-1} in the polyol spectrum. At 1464 cm^{-1} a characteristic absorption band is presented for angular deformation in the plane of the C–OH bond and the formation of the polyol was also verified by the disappearance of the signals at 1656 and 3008 cm^{-1}, which are related to unsaturation of fatty acid chains.[4,22]

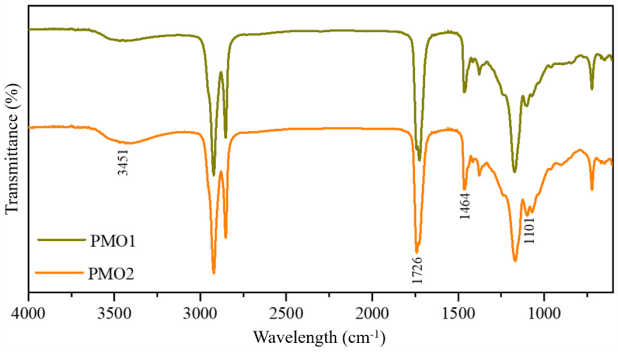

Figure 2. FTIR-ATR spectra obtained for PMO1 and PMO2.

The molecular weight patterns of PMO1 and PMO2 (Table 1) were assessed via GPC analysis, focusing on average number (Mn) and average molecular weight (Mw) using a polystyrene standard. The polydispersity index (PDI) was calculated as PDI = Mw/Mn.[23] GPC chromatograms for both polyols were multimodal. A comparison revealed a higher relative quantity of higher-order oligomers (lower retention time) in PMO2 compared to PMO1, which was determined by the GPC schedule area percentages.[19] In this sense, these oligomers are likely by-products of transesterification and ring-opening polymerization reactions of the epoxide group, where newly formed secondary hydroxyl groups may also react with epoxides.[18,24] The observation of a greater amount of oligomers in PMO2 implies that the polymerization of the epoxide group predominantly led to secondary reactions.

The ^1H NMR spectra (500 MHz, $CDCl_3$) for both oils contain the typical vegetable oils signals, drawn from a to h,

Table 1. Gel permeation chromatography (GPC) results of the obtained polyols, PMO1 and PMO2

Sample	time / min	Mn / Dalton	Mw / Dalton	Area / %	PDI
PMO1					
Fraction 01	15.89	3677	3735	2.99	1.02
Fraction 02	16.73	1599	1671	26.59	1.04
Fraction 03	18.19	460	470	8.07	1.02
Fraction 04	19.67	137	143	21.19	1.04
Fraction 05	20.60	60	61	41.16	1.01
PMO2					
Fraction 01	16.71	1797	1820	3.97	1.01
Fraction 02	17.25	1067	1078	2.93	1.01
Fraction 03	18.20	477	486	8.63	1.02
Fraction 04	19.68	136	138	4.47	1.01
Fraction 05	20.78	51	54	80.00	1.04

PMO1: polyol synthesized from *Moringa oleifera* oil (MO1); PMO2: polyol synthesized from *Moringa oleifera* oil (MO2); Mn: number average molar mass; Mw: weighted average molar mass; PDI: polydispersity index.

representing different types of hydrogen (Table 2) and their corresponding signals.[25]

Regarding the polyols (Figure 3), the signals related to unsaturations (1.98-2.02 and 5.26-5.40 ppm) completely disappeared, while the signal between 5.20 and 5.26 ppm persisted. Hydrogen signals attributed to the formate group (HCOO–, 8.15 ppm) and methine protons linked to hydroxyl and formate groups (–CH(OH), 3.8-4.2 ppm) appeared.[11,25-27] After the epoxidized oil ring opening, it was observed for PMO2 the appearance of a singlet at 2.08 ppm (around 3.1 ppm) attributed to the proton attached to the hydroxyl group.[28] This was more evident for PMO2, confirming a higher oil-to-polyol conversion compared to PMO1.

Table 2. Chemical shifts obtained from ^{1}H NMR (500 MHz, $CDCl_3$) spectrum of oils

Signal	δ / ppm	Identification	Functional group
a	5.26-5.40	olefinics	C**H**=C**H**–
b	5.20-5.26	methine	–C**H**OCOR
c	4.10-4.32	methylene	–C**H**$_2$OCOR
d	2.33-2.38	α-methylene	–OCO–C**H**$_2$–
e	1.94-2.14	allylic methylene	–C**H**$_2$–CH=CH–
f	1.52-1.70	β-methylene	–OCO–CH$_2$–C**H**$_2$–
g	1.22-1.42	methylene	(C**H**$_2$)n
h	0.86 and 0.89	methyl	(–C**H**$_3$)

δ: chemical shift.

In the TGA and its derivative (DTG) (Figure 4), distinct thermal behaviors were observed for MO1 and MO2. MO1 exhibited an initial thermal event between 30 and 113 °C, resulting in a minor mass reduction of 0.48%, attributed to water content expulsion. In contrast, MO2 showed this event between 66 and 130 °C, with a slightly higher mass loss of 0.70%. A second degradation step occurred between 181 and 405 °C, with mass losses of 91.21% for MO1 and 93.00% for MO2. This decomposition likely involves organic matter, including protein components, present in *Moringa oleifera* oil. The remainder of mass loss, between 300 and 428 °C, likely includes fatty acids such as oleic acid, corroborating results with different mass loss percentages (Table S2, SI section). The third stage,

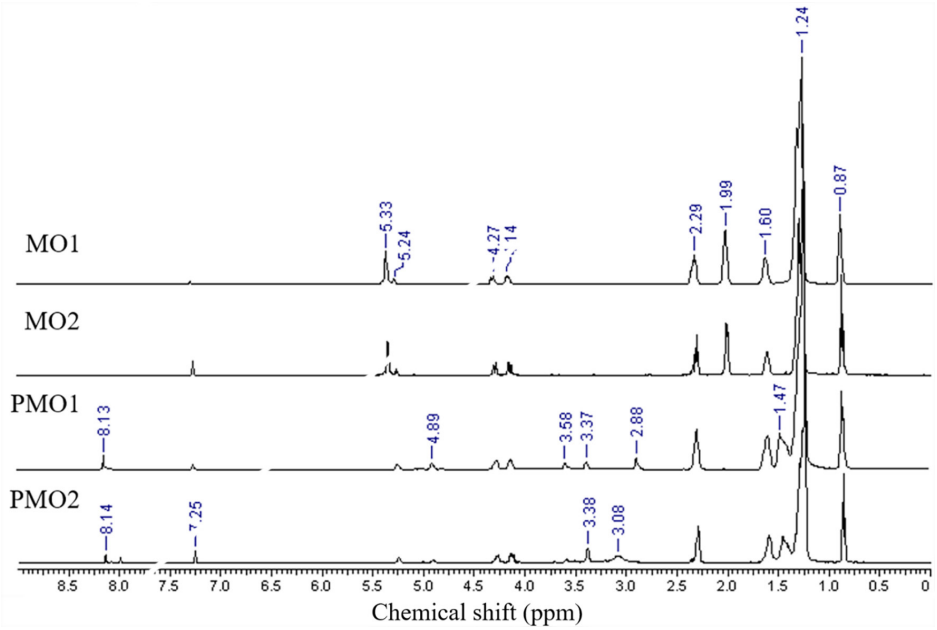

Figure 3. ^{1}H NMR (500 MHz, $CDCl_3$) spectra for MO1, MO2, PMO1 and PMO2.

associated with impurity decomposition, occurred between 405 and 500 °C, with mass losses of 8.63% for MO1 and 5.50% for MO2.[29,30]

The differences between the thermogravimetric curves of MO1 and MO2 verify the heterogeneity of the samples, since the intermediates formed are a mixture of several components, especially due to the difference in the amount of higher molecular weight carboxylic acids, which degrade at higher temperatures.[30,31] Furthermore, Garcia *et al.*[32] explain that the results of thermal stability may be related to the degree of unsaturation of the specific fatty acids in the oils. Typically, the greater the amount of unsaturation, the lower the thermal stability, due to the lower boiling point of saturated fatty acids compared to their saturated counterparts, and therefore, greater amounts of saturated fatty acids in MO2 (Table S2, SI section) increase the thermal stability of this oil and shifting the mass loss process to higher temperatures.

The thermal analysis curves of the polyols (Figure 5) show practically the same four stages of thermal decomposition, but the mass losses occur in different temperature ranges. The decomposition processes of polyols occur in a range of up to 600 °C. PMO2 presents a possible fifth and sixth event, associated with a stage of degradation of the hydroxyl groups present in the polyol, which may be due to the greater presence of hydroxyl groups in PMO2 compared to PMO1.[33] Thus, between 495 and 579 °C, reveal a mass loss of 5.22% (Table S3, SI section). The total weight loss for both polyols was around 98%, while the oils completely degraded.[34]

The DSC thermograms indicate significant differences in the evolution of oils to corresponding polyols. MO1 exhibited the highest crystallization temperature around −10 °C (Table S4, SI section), attributed to triacylglycerols containing mainly saturated fatty acid residues. The peak at approximately −30 °C suggests crystallization of triacylglycerols with unsaturated fatty acid residues.[5,35] The lower unsaturation level in MO2 (67.11% compared to 79.87% in MO1) resulted in a higher value for the most intense Tpeak (−8.54 °C).[36] Triunsaturated triacylglycerol molecules, crystallizing at temperatures as low as −52.66 °C, likely contribute to the strong transition observed below −40 °C for MO1.[37] Thus, different crystallization temperatures in polyols may be related with various crystalline polymorphs, possibly influenced by oligomers in the composition.[35] Both polyols

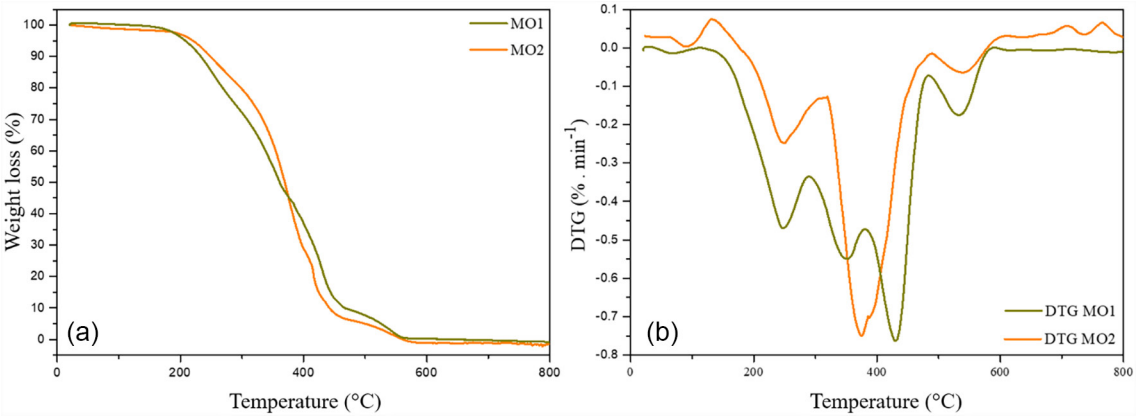

Figure 4. TGA (a) and DTG (b) curves of the extracted *Moringa oleifera* oils.

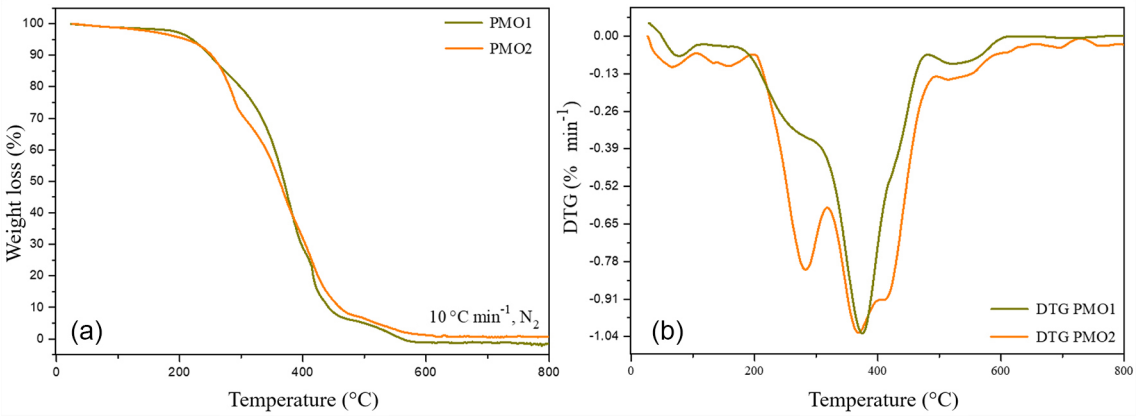

Figure 5. TGA (a) and DTG (b) curves of the synthesized *Moringa oleifera* polyols.

behaved similarly to their respective oils, with PMO2 exhibiting higher melting and crystallization temperatures, represented by broader peaks.[15]

Characterization of polyurethanes (PU1 and PU2)

The reaction mechanism proposal for the polyurethane synthesis was added in the SI section (Figure S1).

PU1 0.4 did not solidify (Figure S4, SI section), due to the [NCO]/[OH] molar ratio being lower than the necessary for the production of the polymeric matrix.[4] The color of this material, although it has a lower [NCO]/[OH] ratio, became darker because after 24 h, at 60 ºC, we left it for another 24 h at 100 ºC, to be sure whether the temperature was correct or not, influencing the polymerization process. The other three PU1 molar ratios ([NCO]/[OH] 0.6, 0.8 and 1.0) presented a similar appearance, showing transparency traits and becoming darker, as well as, less flexible as the [NCO]/[OH] ratio increased. The PU2 was opaque and more rigid, compared to the PU1. The PU2 opacity varied in correspondence with the precursor polyol (PMO2) opacity, which is higher than the PMO1 opacity (Figure S3, SI section).

Figure 6 compares the FTIR spectra of the PU1 with molar ratio [NCO]/[OH] = 0.4 and 1.0 (Figures 6a and 6b, respectively), both freshly synthesized and also after 24 h in an oven at 60 ºC, to verify whether the time and temperature used for curing were sufficient for the effective polymerization of the materials. The PU1-0.4 spectrum after 24 h was almost unchanged compared to the respective spectrum before curing (freshly synthesized). For PU1-1.0 spectrum after 24 h (Figure 6b), the broad absorption band at 3429 cm^{-1}, which appears as the cure progresses, is attributed to the N–H stretching vibration, which confirms the formation of urethane and urea.[38] Another observation is that no peak appeared at 2274 cm^{-1} for the aromatic –NCO– vibration group and at 3530 cm^{-1} for the –OH stretching vibration group, confirming the absence of the –NCO– and –OH group in PU1-1.0. The absence of these two peaks confirms that all –OH groups present in the modified polyol were consumed with isocyanate to form a urethane bond in PU1-1.0, showing that the ratio [NCO]/[OH] greater than 0.4 is more appropriate for obtaining effectively polymerized PU.[3,39]

Theoretically, equal amounts of monomers, i.e., polyol (–OH) and isocyanate (–NCO) are required for the complete polymerization reaction. The study showed that PU at a molar ratio of less than 0.4, as shown in Figure S4 (SI section), did not solidify, establishing that to obtain PU from *Moringa oleifera* polyol, the ratio [NCO]/[OH] greater than 0.4 is more appropriate for obtaining effectively polymerized PU.[4]

The TGA and DTG curves for PU1 with molar ratio [NCO]/[OH] = 0.6, 0.8 and 1.0 are shown in Figure 7. The relevant data are summarized in Table S5 (SI section). All curves exhibited, according to the expected, a three-stage thermal degradation process.[27]

In the first step of degradation of the PUs, the thermogravimetric rate decreased with the reduction of the isocyanate content before 350 °C, which was attributed to the decomposition of urethane portions of PU, therefore accompanied by the release of products derived from TDI. In the second stage, the thermal mass loss rate increased with the reduction of the isocyanate index from approximately 350 to 450 °C, which was mainly attributed to the decomposition of the hydrocarbon chains of the polyol. Decomposition close to 470 °C refers to irregular crosslinking reactions. The third step of thermal degradation with mass loss in the range of 10-12% refers to the waste material. Due to the increase in the isocyanate index in the reagents, which leads to more crosslinking reactions in the last stages of thermal decomposition, it results in

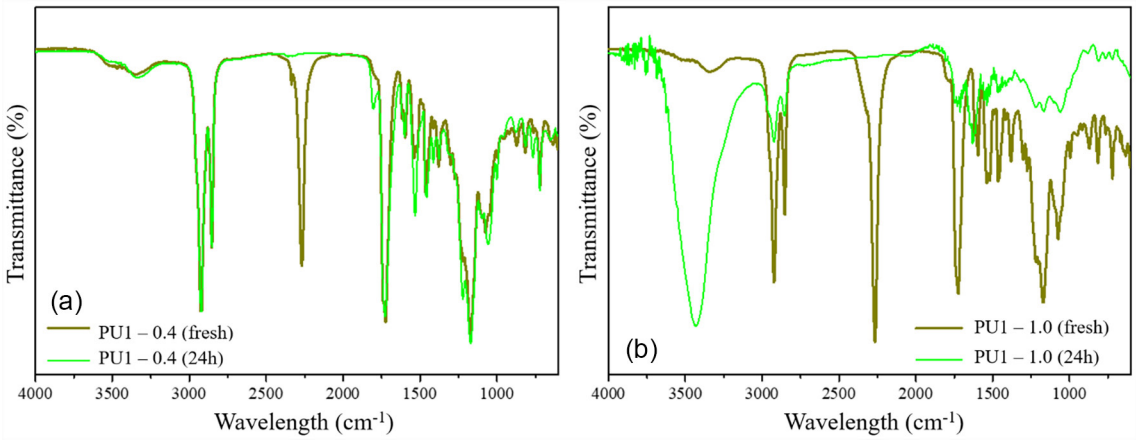

Figure 6. FTIR spectra (fresh synthesized-ATR and after 24 h under 60 °C-KBr) for: (a) PU1-0.4 and (b) PU1-1.0 (PU1-0.4 and PU1-1.0 correspond to PUs synthesized from PMO1 with [NCO]/[OH] molar ratios, respectively, 0.4 and 1.0).

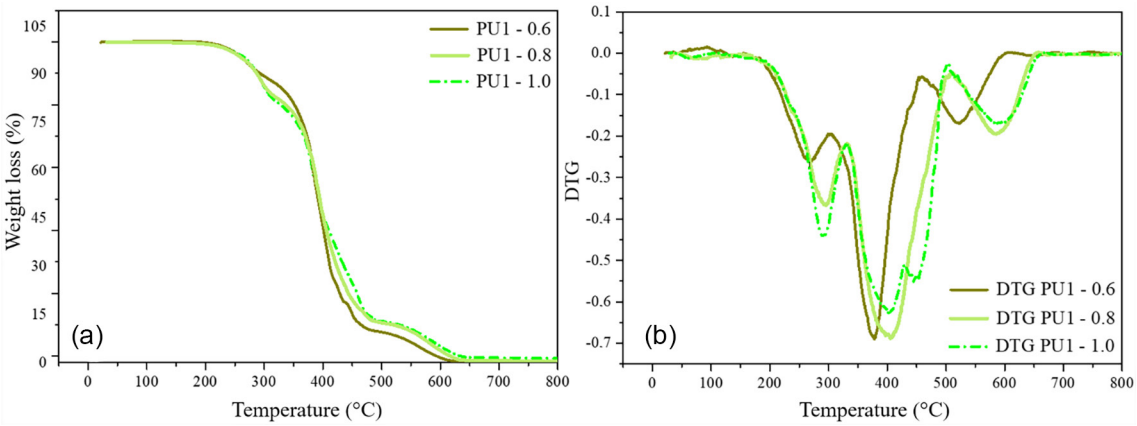

Figure 7. TGA (a) and DTG (b) curves of polyurethanes obtained from PU1 with molar ratio [NCO]/[OH] = 0.6, 0.8 and 1.0.

an increase in the final residue, therefore, the lower the isocyanate index, the lower the residual percentage.[27,40-42] In general, the thermal stability of PUs strongly depends on the urethane groups *per* unit volume, so an increase in the initial mass loss was observed as a function of the increase in the number of urethane groups.[13] Eighty percent mass loss occurred at 433, 446 and 458 °C for PU1-0.6; PU1-0.8 and PU1-1.0, respectively.

The TGA and DTG analyses for the PUs obtained from PMO2 with molar ratio [NCO]/[OH] = 1.0 and 1.2 are presented in Figure 8 and the corresponding data are summarized in Table S6 (SI section).

The PMO2-based PUs also showed three standard degradation steps. First, the degradation related to the urethane bonds, then the polyols contributed to the degradation at higher temperatures, and third, further degradation concerning the fragments produced after the second stage.[43] As shown in Table S6 (SI section), both PUs exhibited the same mass losses.

However, comparing the PUs synthesized with the same molar ratio (PU1-1.0 and PU2-1.0), the mass loss at the first stage was close, but in the other ranges, the data point to a lower thermal stability of PU2-1.0, a behavior explained by the greater thermolability of the precursor polyol (PMO2), although the TGA results have indicated its higher stability compared to PMO1.[44] Furthermore, the temperature of the maximum decomposition rate (Tpeak) follows the same trend, being higher for the PMO1-based PUs. By comparison, the PU1-1.0 sample (Tpeak 291, 403 and 594 °C; Table S5, SI section) is the one with the highest thermal stability, compared to the PU2-1.0 sample (Tpeak 274, 386 and 558 °C; Table S6, SI section), less thermally stable, suggesting that occurred a greater degree of crosslinking for PMO1-based PUs.[20] The initial degradation temperatures (Tonset) of the PUs are presented in Table S7 (SI section), higher for PU1-1.0 compared to PU2-1.0.

DSC analysis (Figure 9) of the PU1s was conducted to observe subtle phase shifts caused by the effect of adding TDI on the PUs. One of the distinguishing features of PUs is the arrangement of hard and soft segments that can be found in their macromolecules. The urethane group in PU acts as a hard domain that enhances the thermal properties of the material, while the long polymeric chain acts as a soft segment in the structure. The soft and hard segments can act as independent structures and therefore both second-order transitions (Tg) and soft segment fusion

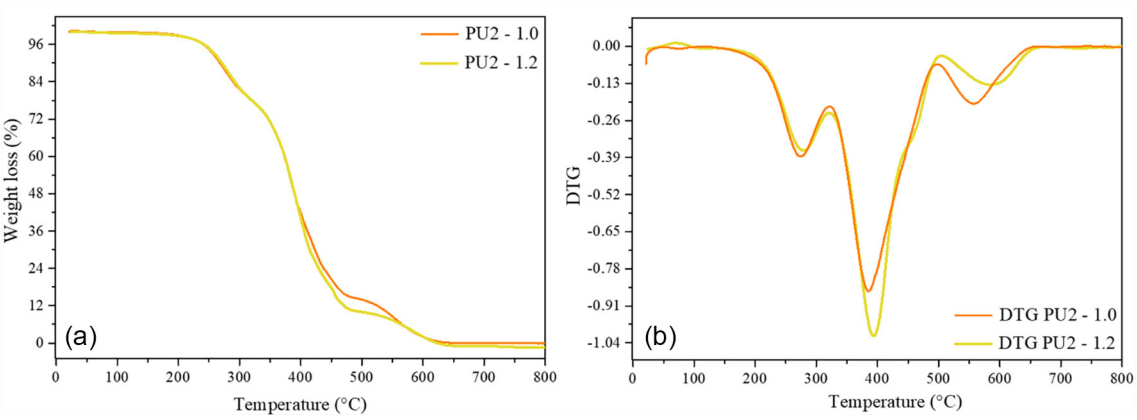

Figure 8. TGA (a) and DTG (b) curves of polyurethanes obtained from PMO2 with molar ratio [NCO]/[OH] = 1.0 and 1.2.

(Tms) or hard segment fusion (Tmh) can appear in the DSC curves.[45] Segmented PUs are typically characterized by three transitions related to the soft segment glass transition, the hard segment glass transition, and the hard phase fusion.

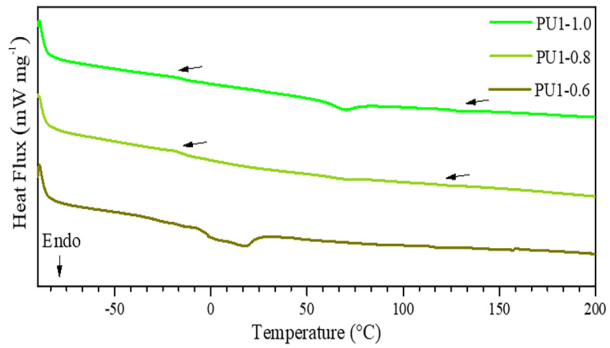

Figure 9. DSC thermograms of polyurethanes obtained from PMO1.

Thus, the DSC curves for PU1-0.8 and PU1-1.0 exhibited three transitions: a glass transition at −18.45 and −18.83 °C (Tg_1), an endothermic melt at 69.18 and 70.61 °C, and a second transition at 122.41 and 129.93 °C (Tg_2). In this sense, Tg_1 relates to the soft segment, while Tg_2 indicates the hard segment, suggesting phase segregation as reported in previous studies.[3] The endothermic peak in PMO1 at −36.82 °C (Table S4, SI section) confirms the melting of the crystalline phase in the soft region, as the melting of the hard segment is due to the melting of the TDI segments at higher temperatures.[14,46]

PU1 with molar ratio [NCO]/[OH] = 0.6 presented a distinct profile, possibly due to fewer crosslinking points, which may impact successful crosslinking. Intermolecular hydrogen bonding of PUs results in successful crosslinking, decreasing chain mobility and increasing the Tg value, this way, the higher [NCO]/[OH] ratio in PU1-1.0 facilitates secondary reactions, contributing to a higher Tg value compared to PU1-0.8.[3,14]

Concerning the DSC curves of the PUs obtained from PMO2 (Figure 10), it is observed that PU2-1.0 and PU2-1.2 presented the same profile as the PUs obtained

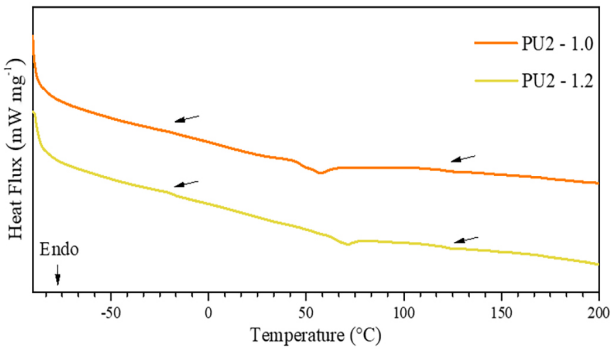

Figure 10. DSC thermograms of polyurethanes obtained from PMO2.

from PMO1, showing that phase segregation also occurs between the domains of the soft and hard segments, due to the existence of two Tgs, with glass transition at −18.67 and −21.15 °C (Tg_1), endothermic melting at 57.24 and 71.44 °C, and a second transition at 123.88 and 124.39 °C (Tg_2).[3]

The DSC results of PU1-1.0 and PU2-1.0 align with the TGA findings for these materials. The greater thermal stability observed for PU1-1.0 suggests a higher degree of crosslinking in the PUs derived from PMO1, leading to fusion of the hard TDI segments at higher temperatures.[14,46] This accounts for the higher transition values seen in PU2-1.2, while no significant difference was observed compared to PU2-1.0, unlike the contrast between PU1-1.0 and PU2-1.0. Thus, the higher molar ratio NCO/OH of 1.2 introduced more crosslinking points, promoting successful intermolecular hydrogen bonding, enhancing chain mobility, and increasing the Tg value. Also, the greater amount of isocyanate for the production of PU2-1.2 may have facilitated secondary responses, contributing to a higher Tg value.[3,14,47]

The mechanical properties of PUs obtained from PMO1 and PMO2 were measured by tensile tests. Tensile strength, elastic modulus (Young's modulus), ultimate stress and ultimate elongation obtained from these curves are summarized in Table S8 (SI section). Modulus of elasticity was extracted from 0 to 5% stress. Modulus of elasticity are linearly correlated with [NCO]/[OH] ratios. Higher [NCO]/[OH] ratios lead to higher modulus of elasticity (less elastic material), consistent with the expected functions of hard and soft segments.[48] It can be seen that the [NCO]/[OH] values affect the mechanical properties, and as the [NCO]/[OH] value of the PUs increased, the tensile strength was improved. However, compared to the tensile strength, the elongation at break of the PUs gradually decreased with increasing [NCO]/[OH] value, making the PUs more rigid.[38,49,50] The two main reasons for this result are that when the value of [NCO]/[OH] increases, the degree of crosslinking of the molecular chains of the PU will be increased and the interaction of the molecular chains will become stronger, thus, the tensile strength of the PU is improved and the elongation at break becomes less. On the other hand, with an increase in the [NCO]/[OH] value, the hard segment content of the PU molecular chain will increase, leading to the stiffness of the PUs, and improving the tensile strength. In contrast to this, the soft segment content decreases with increasing [NCO]/[OH] value, which may reflect on the flexibility of the PUs, reducing the elongation at break.[51]

A possible explanation for the large difference in the elongation at break between the correlates PU1-1.0

and PU2-1.0 is the higher concentration of oligomers in PMO2. The oligomeric compounds in the polyol can act as plasticizers in the PU network, giving rise to a higher elongation at break.[19]

Scanning electron microscopy of the surfaces of the PUs found, PU1 (Figure S7, SI section) and PU2 (Figure S8, SI section), showed morphological and topographical differences; pores of non-uniform diameter, blisters and grooves varied in size and quantity. The surface of PU1-0.6 (Figures S7a-S7c, SI section) presents many grooves, while on the surfaces of PU1-0.8 (Figures S7d-S7f, SI section) and PU1-1.0 (Figures S7g-S7i, SI section), there is the presence of larger bubbles, with a smooth and spherical shape, which were more strongly erupted in PU1-1.0. It is generally admitted that water, which does not contain polyols, reacts predominantly with isocyanate to give carbon dioxide (CO_2) in the initial stage of occurrence; which explains the presence of bubbles in the materials obtained.[52] In the continuous portion of the three PU1s, it was shown a flat and uniform surface; however, in PU1-1.0 it presented a greater quantity of clearer granular structures, suggestive of residual artifacts of the material.[53] The PU2s (PU2-1.0 and PU2-1.2) showed significant differences in the morphology of the external and lateral surfaces. PU2-1.0 (Figures S8a-S8b, SI section) presented a rougher, irregular surface, with smooth cracks, while PU2-1.2 (Figures S8d-S8e, SI section) presented a rougher surface. An apparent closed cell structure can be observed in PU2-1.2 (Figure S8, SI section).[54,55] On their side (Figures S8c and S8f, SI section) there is the presence of wells, formed by bubble structures that formed during the release of CO_2, which are more interconnected with a greater presence of holes in PU2-1.2, when compared to PU2-1.0.[56]

Conclusions

In conclusion, the employed characterization techniques effectively validated the hydroxylation method utilizing *in situ* generated performic acid for the conversion of *Moringa oleifera* oil into polyols. ^{1}H NMR analysis showed that the hydroxyl conversion of the reaction intermediate (oxirane ring) was more effective for MO2. Gel permeation chromatography results showed a higher presence of oligomers in PMO2 compared to PMO1. The results of infrared, thermogravimetric analysis and differential scanning calorimetry of the polyols collectively corroborated with the previous results, which reflected a higher hydroxyl band (FTIR) and higher thermal stability (TGA and DSC) for PMO2. Remarkably, the thermal stability of the *Moringa oleifera* oils was enhanced post-conversion into polyols, aligning with established literature. The obtained PUs also showed a degradation profile compatible with pure PU, without the use of chain extenders and fillers for the formation of composites. Greater thermal resistance was expected for the PU2s.

The mechanical behavior aligned with expectations, as indicated by the increasing isocyanate-to-hydroxyl ratio. The mechanical resistance was evaluated through tensile testing, which illustrated the influence of varying TDI and polyol on the elasticity modulus of PU. The modulus increased as the [NCO]/[OH] ratio decreased, attributed to a reduction in the number of rigid segments and crosslinking density in the material. Additionally, in the polymerization reaction of materials with higher TDI concentrations, there was a greater production of CO_2 gas, leading to increased cavity formation, resulting in a more brittle and less elastic PU.

In essence, this study successfully demonstrated the feasibility of synthesizing PUs from *Moringa oleifera* polyols but still did not suggest a specific application. Future investigations demand additional characterizations of the starting oils and polyols. Furthermore, by incorporating alternative raw materials and meticulous proportion optimization, the potential to engineer PUs with enhanced properties emerges as a promising research field.

Supplementary Information

Supplementary information is available free of charge at http://jbcs.sbq.org.br as PDF file.

Acknowledgments

The authors would like to thank Central Analítica-UFC/CT-INFRA/MCTI-SISNANO/CAPES for their contribution, CAPES and CNPq through the Laboratory of Polymers and Materials Innovation and Embrapa Semiárido. This work was financial supported in part by the Coordination for the Improvement of Higher Education Personnel - Brazil (CAPES) - Financial Code 001, Fundação de Amparo à Pesquisa do Estado de Ceará (Funcap), Edital 01/2022 (No. 07001452/2022/2022) - Mulheres na Ciência and Edital 02/2022 (No. 10592660/2022) - Cooperação Internacional FUNCAP/INSA Rouen Normandie). N.M.P.S. Ricardo thanks CNPq for the research grant (No. 309795/2021-4).

Author Contributions

Kamilla B. Silveira was responsible for conceptualization, investigation, methodology, formal analysis, visualization,

writing original draft; Gabriel É. P. Almeida for investigation, methodology, formal analysis; Debora H. A. de Brito for investigation, methodology, formal analysis; Francisco Alessandro M. Rodrigues for investigation, methodology, formal analysis; Alexandre C. C. Sousa for investigation, methodology, formal analysis, writing review and editing; Elano N. Ferreira for formal analysis; Adriano L. A. Mattos for formal analysis, investigation; Denise R. Moreira for conceptualization, formal analysis, investigation, writing review and editing; Douglas de Britto for formal analysis, investigation; Nágila M. P. S. Ricardo for conceptualization, investigation, writing review and editing, supervision, project administration, and funding acquisition.

References

1. Rayunga, M.; Aunga, M. M.; Ahmadd, A.; Su'aite, M. S.; Abdullaha, L. C.; Jamil, S. N. A. M.; *Mater. Chem. Phys.* **2019**, *222*, 110. [Crossref]
2. Jin, X.; Dong, J.; Guo, X.; Ding, M.; Bao, R.; Luo, Y.; *Poly. Int.* **2022**, *71*, 1384. [Crossref]
3. Shirke, A. G.; Dholakiya, B. Z.; Kuperkar, K.; *Surf. Interfaces* **2019**, *15*, 180. [Crossref]
4. Quirino, R. L.; da Silva, T. F.; Payne, A.; Lopes, R. V. V.; Paterno, L. G.; Sales, M. J. A.; *Coatings* **2015**, *5*, 527. [Crossref]
5. Zhong, J.; Wang, Y.; Yang, R.; Liu, X.; Yang, Q.; Qin, X.; *Ind. Crops Prod.* **2018**, *120*, 1. [Crossref]
6. Salama, M. A.; Harkaoui, S. E.; Nounah, I.; SakR, H.; Abdin, M.; Owon, M.; Osman, M.; Ibrahim, A.; Charrouf, Z.; Matthäus, B.; *OCL: Oilseeds Fats, Crops Lipids* **2020**, *27*, 53. [Crossref]
7. Wiltshire, F. M. S.; Santos, A. F.; Silva, L. K. B.; de Almeida, L. C.; Freitas, L. S.; Lima, A. S.; Fricks, A. T.; Dariva, C.; Soares, C. M. F.; *Food Chem.: Mol. Sci.* **2022**, *4*, 100068. [Crossref]
8. Salama, M. A.; Owon, M.; Osman, M.; Ibrahim, A.; Matthäus, B.; *J. Food Meas. Charact.* **2020**, *14*, 2220. [Crossref]
9. Lligadas, G.; Ronda, J. C.; Galià, M.; Cádiz, V.; *Polymers* **2010**, *2*, 440. [Crossref]
10. Yaakob, Z.; Min, A. M.; Kumar, M. N. S.; Kamarudin, S. S. K.; *J. Thermoplast. Compos. Mater.* **2010**, *23*, 447. [Crossref]
11. Omonhinmin, C.; Olomukoro, E.; Ayoola, A.; Egwim, E.; *AIMS Energy* **2020**, *8*, 102. [Crossref]
12. Monteavaro, L. L.; da Silva, E. O.; Costa, A. P. O.; Samios, D.; Gerbase, A. E.; Petzhold, C. L.; *J. Am. Oil Chem. Soc.* **2005**, *82*, 365. [Crossref]
13. Venkatesh, D.; Jaisankar, V.; *Mater. Today: Proc.* **2019**, *14*, 482. [Crossref]
14. *MestReNova LITE*, version 8.0; Mestrelab, Spain, 2017.
15. Gu, R.; Konar, S.; Sain, M.; *J. Am. Oil Chem. Soc.* **2012**, *89*, 2103. [Crossref]
16. Ekkaphan, P.; Sooksai, S.; Chantarasiri, N.; Petsom, A.; *Int. J. Polym. Sci.* **2016**, *2016*, ID 4909857. [Crossref]
17. Moreira, D. R.; Chaves, P. O. B.; Ferreira, E. N.; Arruda, T. B. M. G.; Rodrigues, F. E. A.; Câmara Neto, J. F.; Petzhold, C. L.; Maier, M. E.; Ricardo, N. M. P. S.; *Ind. Crops Prod.* **2020**, *158*, 112937. [Crossref]
18. Pan, X.; Webster, D.; *ChemSusChem.* **2012**, *5*, 419. [Crossref]
19. Kong, X.; Liu, G.; Qi, H.; Curtis, J. M.; *Prog. Org. Coat.* **2013**, *76*, 1151. [Crossref]
20. ASTM D1957-86: *Standard Test Method for Hydroxyl Value of Fatty Oils and Acids*, West Conshohocken, 1986.
21. Enderus, N. F; Tahir, S. M.; *Mater. Sci. Eng.* **2017**, *271*, e12062. [Crossref]
22. Hejna, A.; Kirpluks, M.; Kosmela, P.; Cabulis, U.; Haponiuk, J.; Piszczyk, Ł.; *Ind. Crops Prod.* **2016**, *95*, 113. [Crossref]
23. Laube, T.; Weisser, J.; Berger, S.; Börner, S.; Bischoff, S.; Schubert, H.; Gajda, M.; Bräuer, R.; Schnabelrauch, M.; *Mater. Sci. Eng., C* **2017**, *78*, 163. [Crossref]
24. Caillol, S.; Desroches, M.; Boutevin, G.; Loubat, C.; Auvergne, R.; Boutevin, B.; *Eur. J. Lipid. Sci. Technol.* **2012**, *114*, 1447. [Crossref]
25. Lopes, R. V. V.; Zamian, J. R.; Resck, I. S.; Sales, M. J. A.; dos Santos, M. L.; da Cunha, F. R.; *Eur. J. Lipid. Sci. Technol.* **2010**, *112*, 1253. [Crossref]
26. Jayavani, S.; Sunanda, S.; Varghese, T. O.; Nayak, S. K.; *J. Clean. Prod.* **2017**, *162*, 795. [Crossref]
27. Chan, Y. Y.; Ma, C.; Zhou, F.; Hu, Y.; Schartel, B.; *Polym. Degrad. Stab.* **2021**, *191*, 109656. [Crossref]
28. Uprety, B. K.; Reddy, J. V.; Dalli, S. S.; Rakshit, S. K.; *Bioresour. Technol.* **2017**, *235*, 309. [Crossref]
29. Barbosa, M. S.; Freire, C. C. C.; Mota, D. A.; Almeida, L. C.; Souza, R. L.; Pereira, M. M.; Lima, A. S.; Soares, C. M. F.; J.; *Bioeng. Technol. Apllied Health* **2020**, *3*, 341. [Crossref]
30. Bhutada, P. R.; Jadhav, A. J.; Pinjari, D. V.; Nemade, P. R.; Jain, R. D.; *Ind. Crops Prod.* **2016**, *82*, 74. [Crossref]
31. Maciel, S. T. A.; Reis, J. H. C.; da Silva, G. F.; Freitas, L. S.; *Braz. J. Chem. Eng.* **2021**, *38*, 23. [Crossref]
32. Garcia, C. C.; Franco, P. I. B. M.; Zuppa, T. O.; Antoniosi Filho, N. R.; Leles, M. I. G.; *J. Therm. Anal. Calorim.* **2007**, *87*, 645. [Crossref]
33. Contreras, J.; Valdés, O.; Mirabal-Gallardo, Y.; de la Torre, A. F.; Navarrete, J.; Lisperguer, J.; Durán-Lara, E. F.; Santos, L. S.; Nachtigall, F. M.; Cabrera-Barjas, G.; Abril, D.; *Eur. Polym. J.* **2020**, *128*, 109606. [Crossref]
34. Abril-Milán, D.; Valdés, O.; Mirabal-Gallardo, Y.; de la Torre, A. F.; Bustamante, C.; Contreras, J.; *Materials* **2018**, *11*, 2244. [Crossref]
35. Coman, A. E.; Peyrton, J.; Hubca, G.; Sarbu, A.; Gabor, A. R.; Nicolae, C. A.; Iordache, T. V.; Averous, L.; *Eur. Polym. J.* **2021**, *149*, 110363. [Crossref]
36. Sharma, B. K.; Rashid, U.; Anwar, F.; Erhan, S. Z.; *J. Therm. Anal. Calorim.* **2009**, *96*, 999. [Crossref]

37. Marikkar, J. M. N.; Ghazali, H. M.; *Int. J. Food Prop.* **2011**, *14*, 1049. [Crossref]
38. Borrero-López, A. M.; Valencia, C.; Franco, J. M.; *J. Cleaner Prod.* **2020**, *277*, 123367. [Crossref]
39. Sun, N.; Di, M.; Liu, Y.; *Int. J. Biol. Macromol.* **2021**, *184*, 1. [Crossref]
40. Gaikwad, M. S.; Gite, V. V.; Mahulikar, P. P.; Hundiwale, D. G.; Yemul, O. S; *Prog. Org. Coat.* **2015**, *86*, 16. [Crossref]
41. Feng, G. D.; Ma, Y.; Zhang, M.; Jia, P. Y.; Hu, L. H.; Liu, C. G.; Zhou, Y. H.; *Prog. Org. Coat.* **2019**, *133*, 267. [Crossref]
42. Patil, A. M.; Jirimali, H. D.; Gite, V. V.; Jagtap, R. N.; *Prog. Org. Coat.* **2020**, *149*, 105895. [Crossref]
43. Zhang, C.; Ding, R.; Kessler, M. R.; *Macromol. Rapid Commun.* **2014**, *35*, 1068. [Crossref]
44. Fang, Z.; Yang, Z.; Ji, D.; Zhu, N.; Li, X.; Wan, L.; Zhang, K.; Guo, K.; *RSC Adv.* **2016**, *6*, 90771. [Crossref]
45. Popescu, M. C.; Vasile, C.; Macocinschi, D.; Lungu, M.; Craciunescuc, O.; *Int. J. Biol. Macromol.* **2010**, *47*, 646. [Crossref]
46. Mizera, K.; Kirpluks, M.; Cabulis, U.; Leszczyńska, M.; Półkac, M.; Ryszkowska, J.; *Ind. Crops Prod.* **2018**, *113*, 98. [Crossref]
47. Paraskar, P. M.; Prabhudesai, M. S.; Kulkarni, R. D.; *React. Funct. Polym.* **2020**, *156*, 104734. [Crossref]
48. Zhen, L.; Creason, S. A.; Simonovsky, F. I.; Snyder, J. M.; Lindhartsen, S. L; Mecwan, M. M.; Johnson, B. W.; Himmelfarb, J.; Ratner, B. D.; *Biomaterials* **2021**, *279*, 121174. [Crossref]
49. Tran, T. K.; Kumar, P.; Kim, H.-R.; Hou, C. T.; Kim, B. S.; *Polymers* **2018**, *10*, 927. [Crossref]
50. Shen, Y.; He, J.; Xie, Z.; Zhou, X.; Fang, C.; Zhang, C.; *Ind. Crops Prod.* **2019**, *140*, 111711. [Crossref]
51. Dai, Z.; Jiang, P.; Lou, W.; Zhang, P.; Bao, Y.; Gao, X.; Xia, J.; Haryono, A.; *Eur. Polym. J.* **2020**, *139*, 109994. [Crossref]
52. Reignier, J.; Alcouffe, P.; Mechin, F.; Fenouillot, F. J.; *Colloid Interface Sci.* **2019**, *552*, 153. [Crossref]
53. de Moura Neto, F. N.; Fialho, A. C. V.; de Moura, W. L.; Rosa, A. G. F.; de Matos, J. M. E.; Reis, F. S.; Mendes, M. T. A.; Sales, E. S. D.; *Polímeros* **2019**, *29*, 2019029. [Crossref]
54. Cerejo, S. A.; Rahal, S. C.; de Lima Neto, J. F.; Voorwald, F. A.; e Alvarenga, F. C. L.; *Acta Cir. Bras.* **2011**, *26*, 333. [Crossref]
55. Wu, Y.; Xiao, C.; Liu, H.; Huang, Q.; *Chin. J. Chem. Eng.* **2019**, *27*, 935. [Crossref]
56. Wang, C.-S.; Zhang, J.; Wang, H.; He, M.; Ding, L.; Zhao, W.; *Ind. Crops Prod.* **2021**, *163*, 113328. [Crossref]

Submitted: February 9, 2024
Published online: July 12, 2024